Published in final edited form as:

J Phys Chem B. 2016 August 25; 120(33): 8361–8368. doi:10.1021/acs.jpcb.6b02053.

Structure and Dynamics Study of LeuT Using the Markov State Model and Perturbation Response Scanning Reveals Distinct Ion Induced Conformational States

Eliana K. Asciutto[†], **Patrick C. Gedeon**[‡], **Ignacio J. General**[†], and **Jeffry D. Madura**[*,§]

[†]School of Science and Technology, Universidad Nacional de San Martín, CONICET, San Martín, Buenos Aires, Argentina

[‡]Department of Biomedical Engineering, Duke University, Durham, North Carolina 27708, United States

[§]Center for Computational Sciences & Department of Chemistry and Biochemistry, Duquesne University, Pittsburgh, Pennsylvania 15208, United States

Abstract

The bacterial leucine transporter (LeuT), a close homologue of the eukaryote monoamine transporters (MATs), currently serves as a powerful template for computer simulations of MATs. Transport of the amino acid leucine through the membrane is made possible by the sodium electrochemical potential. Recent reports indicate that the substrate transport mechanism is based on structural changes such as hinge movements of key transmembrane domains. In order to further investigate the role of sodium ions in the uptake of leucine, here we present a Markov state model analysis of atomistic simulations of lipid embedded LeuT in different environments, generated by varying the presence of binding pocket sodium ions and substrate. Six metastable conformations are found, and structural differences between them along with transition probabilities are determined. We complete the analysis with the implementation of perturbation response scanning on our system, determining the most sensitive and influential regions of LeuT, in each environment. Our results show that the occupation of sites Na1 and Na2, along with the presence of the substrate, selectively influences the geometry of LeuT. In particular, the occupation of each site Na1/Na2 has strong effects (in terms of changes in influence and/or sensitivity, as compared to the case without ions) in specific regions of LeuT, and the effects are different for simultaneous occupation. Our results strengthen the rationale and provide a conformational mechanism for a putative transport mechanism in which Na2 is necessary, but may not be sufficient, to initiate and stabilize extracellular substrate access to the binding pocket.

[*]**Corresponding Author**, madura@duq.edu.

ASSOCIATED CONTENT

Supporting Information

The Supporting Information is available free of charge on the ACS Publications website at DOI: 10.1021/acs.jpcb.6b02053.

Protein data bank files for the six macrostates (ZIP)

Graphs of implied time scales as a function of lag times; RMSD per residue between macrostates xna2 and sna; RMSD per residue between macrostates xna0 and sna; influence profiles for the whole system between xn and sn; and the six macrostates found from MSM (PDF)

The authors declare no competing financial interest.

Graphical abstract

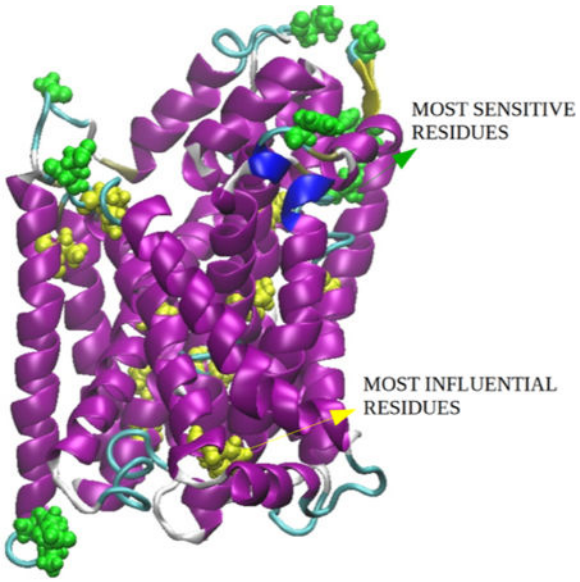

INTRODUCTION

Transmembrane proteins function as gateways to allow the transport of small molecules into cells. Conformational changes in these transmembrane proteins allow the entrance of the small molecules to be transported. These conformational changes may cause, for example, the binding site to be only accessible from one side of the membrane and not from the other. Monoamine transporters (MATs) are a subset of transmembrane proteins that use the electrochemical potential of specific ions to initiate the aforementioned conformational changes. MATs belong to a group of homologous transmembrane proteins that function by Na^+ dependent secondary active transport. MATs are located at the synaptic cleft, allowing for the reuptake of neurotransmitters and the consequent termination of signaling in the chemical synapse.[1]

MATs regulate brain pathways associated with addiction, mood disorders, hypertension, bipolar disorder, and Parkinson's disease.[1–3] Despite the fundamental importance of these transporters and despite the fact that known drugs currently on the market use them as targets, their structure and transport dynamics still remain unknown. The bacterial Na^+ dependent leucine transporter (LeuT) is a close homologue of the MATs. Its X-ray crystal structure was published by Yamashita et al.,[4] and frequently used as a template for computer simulations of MATs.[14–23] In this crystal structure, the amino acid leucine and two Na^+ ions are located in a binding pocket and LeuT is in an outward open conformation. After the LeuT crystal structure was published,[4] several studies appeared supporting the idea of two Na^+ in the same binding pocket.[5,6] In 2008, a new mechanism was proposed, where the occupancy of two different binding sites is essential for the transport mechanism.[7] This proposition sparked a significant controversy. Regarding the transport mechanism, Gouaux's group proposed in a recent work that both, local conformational changes and rigid body movements of groups of helices are associated with the transport mechanism.[8] Following

this concept, the transport of substrate is performed through a series of structural conformational changes.

In this work, we investigate if the structure of LeuT depends on the presence of Na^+ in the binding pocket and how the structure is affected by the presence of substrate and ions. We perform seven accelerated molecular dynamics simulations, one in each environment. Environments are characterized by the presence or absence of leucine substrate and the presence or absence of one or both Na^+ ions. The details of the simulations are explained in the Methods section.

We studied structural differences between environments and their corresponding transitions using two different methods:

1. A Markov state model, as implemented in MSMbuilder2.[10] The conformational space formed by the seven trajectories grouped in a single one is partitioned into discrete small states that are structurally similar. The states found are grouped in macrostates connected through dynamic clusters calculated from an $N \times N$ transition probability matrix. The transition probability matrix consists of the conditional probabilities for the system to be found in state n' at time $t + \delta t$, given that it is in state n at time t. From here, representative states and transitions between them can be calculated. With MSM, it is also possible to identify the relevant dynamics using the assumption that the dynamics can be decomposed into a superposition of m slow dynamical processes and the remaining fast processes. The "slow" dynamics, usually the relevant biological dynamics, can be identified by the first m eigenvalues and eigenvectors of the transition probability matrix. The idea is then to relate metastable states from the MSM model with conformations that populate a specific environment.
2. Perturbation Response Scanning[28] (PRS), a method that allows the calculation of the response of a residue to a perturbation on another one. This is achieved by interpreting the system as an anisotropic network model (ANM[29]), where each residue represents a node of the network, and nodes interact if they are closer than a given cutoff distance (12 Å). PRS was used here to identify the most influential and most sensitive residues of LeuT, when ions and substrate are present or not.

Using these two methodologies, we identify regions affected by the substrate and the ions in different locations.

METHODS

aMD simulation of the lipid-transporter environments was performed as previously reported.[9,13,32,33] In brief, LeuT structure coordinates were obtained from Protein Data Bank entry 2A65 (www.rcsb.org; MMDB accession no. 3495). These coordinates correspond to the "occluded" structure of the bacterial (*Aquifex aeolicus*) leucine transporter protein. Missing nonterminal residues (N133 and A134) were introduced using the model building module in Molecular Operating Environment. [34] Hydrogen atoms and a C-terminal carboxyl group were added using CHARMM 35b1.[35] The resulting protein structure was energy

minimized while holding the crystal coordinates fixed in CHARMM, allowing for correction of any unnatural strain created by the addition of the missing atoms. A protonation state representative of free amino acids in water at a pH of 7 was used. The resulting protein structure including binding pocket substrate and ions was embedded in a 1-palmitoyl-2-oleoyl-*sn*-glycero-3-phosphoethanolamine (POPE) lipid membrane, solvated, heated, and subjected to 30 ns of classic MD simulation as previously reported.[13] In brief, this initial cMD simulation was performed by using NAMD 2.6[38] optimized for a Cray-XT3 computer (Pittsburgh Supercomputing Center) and using the CHARMM27 parameters for proteins and lipids.[39,40] The energy minimized and cMD equilibrated lipid-transporter system served as the starting structure for aMD simulation.[9,32] Seven different environments were created from this starting structure by varying the presence of the binding pocket substrate and sodium ions. Each of the seven different environments underwent 5 ns of cMD equilibration followed by 300 ns of aMD equilibration in AMBER9,[36] as previously described.[32] In brief, each of the seven different environments were simulated with the sander module of AMBER9[41] using the ff99SB force field, with the exception of both the POPE lipid molecules, for which the parameters from AMBER's antechamber and GAFF[41] were used, and the leucine substrate zwitterion where present, for which R.E.D.[42] was used to determine the charges. After 5 ns of cMD equilibration using these parameters, a previously described aMD patch for AMBER[43] was applied to protein atoms within each simulation. This allowed the dihedral potential energy to be boosted when it fell below a predetermined thereshold. The threshold was determined on the basis of energy values obtained during cMD simulation. Specifically, the energy minimum below which acceleration was applied was set to 12620 kcal/mol and the alpha well depth value was set to 2524. Each of the seven different environments underwent aMD simulation for 300 ns at 310 K. The aMD trajectories were later reweighted, in the analysis stage, by assigning a weight to each frame, according to the well-known reweighting factor,[43] $e^{\beta \Delta V[\mathbf{r}(\mathbf{t}_i)]}$, where ΔV is the potential boost used to accelerate the dynamics, which is a function of the coordinates, which, in turn, are functions of time.

Markov State Model (MSM)

Following aMD equilibration, ions, substrate, water, and lipids were removed from the trajectories and the seven aMD trajectories were combined into a single one for MSM analysis. The clustering of the configuration space was done using a hybrid cluster *k*-center algorithm,[10] considering only C_α atoms with a fixed distance of 1.5 Å. The relaxation time scales, which are inversely proportional to their respective eigenvalues, were calculated to ensure independence of the time between frames (lag time). Using the robust Perron cluster analysis (PCCA+), eigenvectors of the conditional probability matrix were calculated to identify invariant subsets of states in the Markovian chain. The obtained microstates were lumped into macrostates and identified according to the environment to which it belongs. Next, a random frame was selected from each of the seven aMD trajectories and subjected to 100 ns of additional cMD simulation. Transition probabilities between macrostates were calculated using these cMD data.

Perturbation Response Scanning (PRS)

The collective dynamics of the system is fully defined by the $3N \times 3N$ covariance matrix (**C**), obtained from the reweighted aMD simulations of the system, where we take each of the N residues to represent a node of the network. Node positions are identified with the coordinates of Cα atoms. The application of a perturbation, a $3N$-dimensional force vector **F**, generates a response of the system, given by the $3N$-dimensional vector **ΔR** of node displacements, which is governed by Hooke's law, $\mathbf{F} = \mathbf{C}^{-1}\mathbf{\Delta R}$. The idea of PRS[28] is to exert a force of a given magnitude on the network, one residue at a time, and observe the response of each of the nodes in the network.

The force exerted on residue i is expressed as

$$\mathbf{F}^{(i)} = (0\,0\,0 \ldots F_x^{(i)} F_y^{(i)} F_z^{(i)} \ldots 0\,0\,0)^T \quad (1)$$

with a corresponding response

$$\mathbf{\Delta R}^{(i)} = \mathbf{C}\mathbf{F}^{(\mathbf{i})} \quad (2)$$

Here, $\mathbf{\Delta R}^{(i)}$ is the $3N$-dimensional vector that describes the deformation of all the residues in response to $F^{(i)}$. By forming the N-dimensional vector containing the square displacement of each residue and collecting all the resulting vectors in a matrix, we obtain the PRS matrix, whose element (i, j) is the square displacement of residue j to a unit perturbation force on residue i. Dividing each element by the diagonal one in its same row, we obtain a normalized PRS matrix, where element (i, j) now represents the square displacement of residue j to a unit displacement at residue i. For the full details of the method, see ref 27.

With this normalization (which is not unique), row i of the matrix forms a vector describing the **influence profile** of residue i on other residues, while column j describes the response or **sensitivity profile** of residue j to perturbation of other residues.

RESULTS AND DISCUSSION

Ions, substrate, water, and the membrane were removed from the trajectories, and the seven trajectories were combined into a single one.

Markov State Model

The partitioning of the configuration space was done using a hybrid cluster k-center algorithm,[10] considering only C_α atoms with a fixed distance of 1.5 Å. From this clustering, 45 conformational states were obtained.

It is important here to evaluate the resulting Markovian character of the model. The relaxation time scales, which are inversely proportional to their respective eigenvalues, should be independent of the time between frames (lag time). Figure S1 in the Supporting Information shows that the slowest process is reaching equilibrium with a lag time of 50 ps.

The value obtained for the slower time scale (10 ns) is amplified by aMD; therefore, we only focus here on a qualitative analysis, noticing that the model is showing convergence and separation between the time scales of the physical processes involved. The observed gaps between time scales also suggest that six macroscopic states will reasonably describe all of the physical processes occurring in the dynamics. Hence, we choose to build our model with six macrostates. With a shorter lag time of 10 ps, kinetical related microstates were lumped into six macrostates using the robust Perron cluster analysis ($PCCA^+$).[11,12] $PCCA^+$ is a spectral cluster algorithm that identifies invariant subsets of states in the Markovian chain, using the eigenvectors of the conditional probability matrix.

The 45 microstates lumped in 6 macrostates are shown in Figure 1. Each microstate has been labeled according to the environment to which it belongs. The presence or absence of substrate is denoted by S or X, respectively. N1 indicates that only $Na1^+$ is present, N2 indicates that only $Na2^+$, and N indicates that both ions are present. The six macrostates are labeled in lowercase using the same criteria. Their respective populations are xna_0: 0.05, xna_1: 0.06, xna2: 0.12, sna2: 0.11, xx: 0.14, and sna: 0.53. We named sna the most populated macrostate, even though it is composed of a mixture of environments: SN1, SN2, SN, XN1, XN2, XN (all except XX). We chose to name it sna because configurations belonging to the SN environment are only found in this specific macrostate.

The structural characteristics of the most populated macrostate (sna) are found in all the environments, except XX. This geometry seems to be the most stable geometry whenever substrate or ions are present. It is very similar to the published occluded structure 2A65,[4] with a RMSD value of 1.11 Å. From the five remaining macrostates, only one belongs to the environment with substrate, and has only $Na2^+$ present (sna2), and the rest correspond to substrate-free environments. To find structural differences due to the presence of substrate and ions, we compare the geometry of the xx macrostate (substrate and ions-free) with the geometry of the five remaining states.

In the core region, several structural differences between macrostates are observed. The extracellular loop 2, EL2, connecting transmembrane domains TM3 and TM4 is rotated closing the outward region for the macrostate sna2 with respect to xx (Figure 2, top). A similar rotation is observed for the macrostate sna. The most salient structural difference in this region is observed for the macrostate xna_0 (both Na sites occupied); for this macrostate, the end of EL2 (residues P137–I140) loses its helical character converting to a turn, increasing therefore the space for a possible substrate entrance (Figure 2, top). An additional region showing structural changes between macrostates is located in the first intracellular loop, IL1, and the end of TM3. In that region, considerable differences exist for the macrostates coming from the environments where both ions are present (SN, XN). For the first substrate-free and both ions-present macrostate (xna_0), IL1 is completely unfolded, leaving TM3 and TM2 connected by a turn structure (Figure 2, bottom right). In sna, the end of TM3 makes a hinge-like movement, forming a new short helix displaced toward the inside region (residues R88–G94) (Figure 2, bottom left). This hinge-like movement could act as an intracellular gate, and consistently with this idea, it is formed when the substrate is present.

Some structural changes between macrostates are also observed at the binding pocket. For the TM1a helix, changes are observed only for the macrostate representing the environment containing $Na2^+$ and no substrate bound (xna2). In this conformation, the upper part of the TM1a helix (residues G20–A22) unfolds, increasing space at the binding pocket (Figure 3).

Right at the outward end of the TM5, the β_1 strand is displaced inward in the sna2 macrostate, partially closing the extracellular region (Figure 4, left). Close to the binding pocket, in the extracellular region, between the TM8 helix and the extracellular loop EL4b, structural changes between macrostates pointing to differences between only the Na2 site occupied and both ions present are observed. For the sna2 macrostate, EL4b is displaced away from TM8 (Figure 4, right). For xna_0 (when both ions are present), TM8 also moves outward, increasing the volume of the binding pocket, with the inward end of the helix making a hinge-like movement (Figure 4, right).

Outside the core, a zone in which structural differences are observed is the 11 transmembrane helix, TM11. The sna2 macrostate differs with xx at the outward end of TM11, where residues K474–E478 make a hinge-like movement resulting in a 45° inward tilt, closing the outward region. Macrostates xna2 and xna_1 have the entire TM11 domain rotated inward about 30° with respect to xx. Surprisingly, the macrostate sna does not have significant differences from the macrostate xx in the TM11 domain. Also significant structural changes are seen at the inward end of the TM12 helix. Macrostates representing environments with only $Na2^+$ present, (sna2 and xna2), have this helix perfectly folded, while for the remaining macrostates the inward end of the helix (residues R509–T515) is unfolded in a coil structure. This observation suggests that $Na2^+$ stabilizes the inward region of the last big helix (TM12).

Following Guoaux,[6] inter-residue distances R5–D369 and R30–D404 can be related with intra- and extracellular gates, respectively. Calculated R5–D369 and R30–D404 sampled by the six macrostates during the simulations are shown in Figure 5. State xna_0 displays the largest intracellular gate distance overall, with an average value similar to the one found in the inward open structure previously reported by our group.[9] More structures can be associated with calculated macrostates: state xna2 to an occluded structure also reported previously by our group,[9] state xx with 3F3A (an outward open conformation), and state sna2 with our initial structure 2A65. It is important to note here that the sampled distances correspond to the frames that conform each macrostate but not the macrostates themselves (in other words, the macrostates are not defining a specific conformation, like the outward or inward facing ones, but a large collection of them).

MSM allows us to calculate the transition probability matrix, which characterizes the kinetics of the system and gives transition probabilities between the macrostates described in the previous section. Transitions between microstates are depicted in Figure 1, represented by single arrows connecting nodes while those between macrostates are represented by double arrows. Probabilities between macrostates were calculated from a new data set generated with standard MD. It consisted of seven trajectories of 100 ns. Each trajectory corresponds to a different environment, and the starting point was for all the cases a random frame from the aMD trajectory. The total simulation time is 700 ns. The most probable

transition toward the most populated state sna corresponds to a transition from macrostate xna2. This result can be interpreted as only the occupation of the Na2 site promotes the required structural changes preparing the binding site to receive the substrate. These structural changes occur in regions TM1a, intracellular loop IL2, extracellular loops EL2, and EL3 (Figure S2). Transition corresponding to the entrance of substrate, once both ions are present, occurs in two steps. It starts in the conformation represented by macrostate xna_1 and jumps to xna_0 with a high transition probability value. Structural differences between xna_1 and xna_0 are observed mainly in the binding site (TM1a), intracellular loops IL2 and IL5, and extracellular loop EL2 (Figure S3, top). Between xna_0 and sna, more changes are observed in intra- and extracellular loops IL2, EL2, and EL4b (Figure S3, bottom). The characteristic structure for sna2 converts readily in the most populated sna, while the opposite transition is much less frequently observed. Macrostate sna2 resembles a structure found in our previous work,[9] named TGM2 (rmsd value 1.31 Å). This result also supports a transport mechanism where $Na2^+$ binds before $Na1^+$.

Transition probability double arrows between xx and the rest of the macrostates are not shown because in the new data set, constructed specifically for the calculation of transition probabilities, a metastable state representing the XX environment is absent. The lack of a metastable xx state can be rationalized by considering that in aMD the probability of transitions between configurations belonging to xx is very low compared with the rest, so it is very likely that considerably more data would be required in standard MD to observe an xx metastable state.

Perturbation Response Scanning

A normalized PRS matrix was calculated for each of the original seven trajectories, so that we could compare the influence and sensibility profiles of different environments. Figure 6 shows the LeuT structure colored by influence (left panel) and sensitivity (right panel). The value of each residue is an average over all the simulated environments. There we can see a usual result of PRS, where the most influencing (blue) residues are located in the core of the system, while the most sensitive ones are found on its exterior. This result can be intuitively comprehended, since surface residues—the most sensitive—are bound only from the inner side of the molecule, not from the exterior, so they are able to move relatively freely, and adapt to the influences of inner, tightly bound core residues. We should also notice that this result is highlighting the importance of the binding pocket, since it is located in the core region, the most influential one. Of course, this was to be expected, being that substrate binding is known to have significant consequences in the structure of LeuT. This also agrees with ref 37, where the author shows that, for SERT—a member of the NSS family which possesses a high sequence identity to LeuT in the binding region—certain residues located in TM1 and TM3, near the substrate's binding site, are highly influential. In fact, cystein mutations in them change the characteristics of the system, protecting it against reagents that would inactivate it otherwise.

Figure 7 shows the difference of the sensibility profiles (i.e., the average response of each residue to perturbations in every other residue of the system) of environment XX with XN1, XN2, and XN in the region close to EL2. It can be seen that both XN1 and XN2 show a

clear difference in the sensitivity of EL2, around N133, as compared to XX. However, this changes for XN, where the peak in sensitivity of EL2 is displaced to V154. This result agrees with the findings of the previous section, represented in Figure 2, where EL2 shows a different orientation in the absence or presence of either Na1, Na2, or both together. PRS adds to this the distinction of a shift in the sensitivity of EL2 when only one (XN1 and XN2) or both (XN) ions are present simultaneously, which could explain the noted loss of helical character in the end of EL2, which in turn increases the space available for the entrance of the substrate.

This also appears to contradict the hypothesis seen in the literature, that only one ion is enough to open the gate; the qualitative PRS response of EL2 is the same for XN1 and XN2, but a clear change is seen in the XN case, with a displaced increase in sensitivity.

Figure 8 shows the difference in the influence profiles of the XX and XN11 environments (left panel) and the XX and SN1 ones (right panel) in the region close to IL1. In both cases, a large difference is observed for the TM3 region. This is in agreement with the MSM fact that shows a break at the beginning of TM3 for the conformations in the sna cluster. From both MSM and PRS, it appears that the $Na1^+$ ion is the cause of this breaking event (since most components of cluster sna and both plots in Figure 8 contain ion $Na1^+$ which, as mentioned before, generates a small separate helix with hinge-like movements that could act as a gate).

It was noted in the previous section, in reference to the lower right panel of Figure 2, that IL1 completely loses its helical structure when going from the XX (neither substrate nor ions) to the xna0 (both ions but no substrate) cluster. This appears confirmed by PRS, as in Figure 9 there is a strong difference in sensitivity between the XX and XN cases, centered around the R86 residue of IL1. Such a change in sensitivity by IL1 could effect a drastic conformational change, as the one noted, and it will have consequences in terms of how information is transmitted between its two sides. Presumably, a higher sensitivity of IL1 in the XN case will result in a tighter connection between the two sides, TM2 and TM3; in fact, this is observed by PRS (not shown) as an increased influence of TM2 on TM3, and vice versa.

A breakage of the helix along TM1a in the XN2 environment (Figure 3) was observed in the MSM analysis. Correspondingly, PRS shows in Figure 10 a large reduction in the influence of that broken helix, around residue A22, and also in the first few residues of TM1b, around L29, expressing a loss of influence of this region, where $Na1^+$ binds, on the rest of the system. At the same time, a significant increase in the sensitivity of the broken portion of the TM1a region is observed, as expected from the fact that this region does not have an organized shape. These results suggest that $Na2^+$ could be a trigger for the system to become sensitive to the influence of $Na1^+$, via the highly sensitive end of TM1a. The breakage of TM1a can also be viewed as a small tilt between structures. The existence of a small tilt in TM1a was previously observed by Kazmier et al.[30] and more recently by Gur et al.[31] In both articles, a small tilt is reported in TM1a between the wild type outward occluded structure and the inward facing occluded crystal structure, in contrast with large tilts observed for some mutants representing the occupancy of Na2.

Finally, Figure 11 demonstrates the increase in the influence of EL4b, and in the sensitivity of both EL4a and EL4b, and TM8. More precisely, the increase in influence is a very specific one, only a few residues around A335, for both environments, SN2 and XN. On the contrary, the increase in sensitivity is very large and extended for XN, comprising mostly all of the residues in EL4b and TM8. The explanation for the latter could be, as in the previous paragraph, that the EL4b and TM8 regions become sensitive when the two Na ions are bound, in order for the system to be ready to transmit the signals coming from the substrate when this one binds. In this way, TM8 and EL4 to a lesser extent act as sensors of the substrate, that can later transmit its influence to the rest of the system.

Conclusions

MSM has been applied to a series of aMD simulations, resulting in the finding of six overall macrostates, containing each one or more environments (Figure 1). From there, specific conformational characteristics typical of each environment were found (Figures 2–4). Next, the application of PRS (Figures 7–11) served to corroborate the importance of the mentioned characteristics.

On the basis of those analyses, the occupation of sites Na1 and Na2, along with the presence of the substrate, influences selectively the geometry of LeuT. In particular, as noted in the previous sections and also in the Supporting Information (Figure S4), we found that the occupation of site Na1 has strong effects (in terms of changes in influence and/or sensitivity, as compared to the case without ions) in EL2, IL1, TM3, TM8, and TM1. Likewise, occupation of Na2 is related to changes in EL2, TM1a, TM8, TM6a, and EL4. Finally, simultaneous occupation of those sites relates to EL2, IL1, EL4b, TM1a, and TM8.

Consideration of Figure S4 shows that the concurrent population of both Na^+ binding sites (environment XN) has a very strong effect in the influence profiles of the system, as compared to the XX environment. However, this effect is drastically reduced when the substrate is also bound. This picture is in agreement with the mechanism that proposes that the binding of two Na^+ ions disturbs the system, leading it to change its conformation to one more predisposed to accept a substrate, whose binding once again re-establishes the influence profile of the system.

This result, along with the observations from the different MSM macrostates, strengthens the rationale and provides a conformational mechanism for a putative transport mechanism in which Na2 is necessary, but may not be sufficient, to initiate and stabilize extracellular substrate access to the binding pocket. This is in partial agreement with previous computational work demonstrating that Na^+ in the Na2 site is required for structural stability of the binding pocket[24] and that the transition of outward- to inward-facing conformations relies heavily on the presence or absence of Na^+ in the Na2 site.[7,25] Furthermore, our results expand upon the role of Na^+ in the Na1 binding site; while previous computational work has demonstrated that Na^+ in the Na1 binding site diminishes outward opening, moving the transporter to an occluded state, here, through the use of extensive aMD calculations, we obtain a more extensive conformational change when two sodium ions are present in the binding pocket, and provide a conformational mechanism by which changes in the intracellular region occur, allowing for substrate reuptake.[26]

Another novel result of the work presented here is the existence of two macrostates (xna_0 and xna_1), each representing a substrate-free environment with both ions present. The average rmsd between these two states is 1.7 Å. The region with the most significant differences is the extracellular loop 2 (EL2) (Figure S1). For state xna_1, EL2 is a helix, while, for xna_0, part of this loop (residues P137–I140) is unfolded in a turn structure. The transition $xna_1 \rightarrow xna_0 \rightarrow$ sna involves then an increase in volume of the binding site through the unfolding of EL2, in order to allow substrate entrance. Both states xna_0 and xna_1 are similar to the outward open conformation 3TT1[8] with rmsd values of 1.54 and 1.51 Å, respectively.

Supplementary Material

Refer to Web version on PubMed Central for supplementary material.

Acknowledgments

This work is supported by the National Institutes of Health, National Science Foundation, Department of Defense, and The U.S. Department of Education under award numbers 5R01DA27806-2, CHE-1005145 (REU/ASSURE), CHE-0723109 (MRI), and P116Z080180. E.K.A. and P.C.G. thank T. J. Lane for assistance with the implementation of MSMbuilder.

References

1. Surratt CK, Ukairo OT, Ramanujapuram S. Recognition of Psychostimulants, Antidepressants, and other Inhibitors of Synaptic Neurotransmitter Uptake by the Plasma Membrane Monoamine Transporters. AAPS J. 2005; 7:E739–E751. [PubMed: 16353950]
2. Ritz MC, Lamb RJ, Kuhar MJ. Cocaine Receptors on Dopamine Transporters are Related to Self-administration of Cocaine. Science. 1987; 237:1219–1223. [PubMed: 2820058]
3. Haapaniemi TH, Ahonen A, Myllylä VV. 123Iβ-CIT SPECT Demonstrates Decreased Brain Dopamine and Serotonin Transporter Levels in Untreated Parkinsonian Patients. Mov. Disord. 2001; 16:124–130. [PubMed: 11215571]
4. Yamashita A, Singh SK, Gouaux E. Crystal Structure of a Bacterial Homologue of Na+/Cl −Dependent Neurotransmitter Transporters. Nature. 2005; 437:215–223. [PubMed: 16041361]
5. Singh SK, Yamashita A, Gouaux E. Antidepressant Binding Site in a Bacterial Homologue of Neurotransmitter Transporters. Nature. 2007; 448:952–956. [PubMed: 17687333]
6. Singh SK, Piscitelli CL, Yamashita A, Gouaux E. A Competitive Inhibitor Traps LeuT in an Open-to-out Conformation. Science. 2008; 322:1655–1661. [PubMed: 19074341]
7. Shi L, Quick M, Zhao Y, Weinstein H, Javitch JA. The Mechanism of a Neurotransmitter: Sodium Symporter- Inward Release of Na. and Substrate is Triggered by Substrate in a Second Binding Site. Mol. Cell. 2008; 30:667–677. [PubMed: 18570870]
8. Krishnamurthy H, Gouaux E. X-ray Structures of LeuT in Substrate- Free Outward-Open and Apo Inward-Open States. Nature. 2012; 481:469–474. [PubMed: 22230955]
9. Thomas J, Gedeon PC, Grant BJ, Madura JD. LeuT Conformational Sampling utilizing Accelerated Molecular Dynamics and Principal Component Analysis. Biophys. J. 2012; 103(1):L1–L3. [PubMed: 22828348]
10. Beauchamp KA, Bowman GR, Lane TJ, Maibaum L, Haque IS, Pande VS. Msmbuilder2: Modeling Conformational Dynamics at the Picosecond to Millisecond Scale. J. Chem. Theory Comput. 2011; 7(10):3412–3419. [PubMed: 22125474]
11. Deuflhard P, Weber M. Robust Perron Cluster Analysis in Conformation Dynamics. Lin. Alg. Appl. 2005; 398:161–184.
12. Kube S, Weber M. A Coarse Graining Method for the Identification of Transition Rates between Molecular Conformations. J. Chem. Phys. 2007; 126:024103. [PubMed: 17228939]

13. Gedeon PC, Indarte M, Surratt C, Madura JD. Molecular Dynamics of Leucine and Dopamine Transporter Proteins in a Model Cell Membrane Lipid Bilayer. Proteins: Struct., Funct., Genet. 2010; 78:797–811. [PubMed: 19899168]
14. Guptaroy B, Zhang M, Bowton E, Binda F, Shi L, Weinstein H, Galli A, Javitch JA, Neubig RR, Gnegy ME. A Juxtamembrane Mutation in the N terminus of the Dopamine Transporter Induces Preference for an Inward-Facing Conformation. Mol. Pharm. 2009; 75(3):514–524.
15. Xhaard H, Backstrom V, Denessiouk K, Johnson MS. Coordination of Na(+) by Monoamine Ligands in Dopamine, Norepinephrine, and Serotonin Transporters. J. Chem. Inf. Model. 2008; 48(7):1423–1437. [PubMed: 18543980]
16. Beuming T, Kniazeff J, Bergmann ML, Shi L, Gracia L, Raniszewska K, Newman AH, Javitch JA, Weinstein H, Gether U, et al. The Binding Sites for Cocaine and Dopamine in the Dopamine Transporter Overlap. Nat. Neurosci. 2008; 11(7):780–789. [PubMed: 18568020]
17. Schlessinger A, Geier E, Fan H, Irwin JJ, Shoichet BK, Giacomini KM, Sali A. Structure-Based Discovery of Prescription Drugs that Interact with the Norepinephrine Transporter, NET. Proc. Natl. Acad. Sci. U.S.A. 2011; 108(38):15810–15815. [PubMed: 21885739]
18. Andersen J, Stuhr-Hansen N, Zachariassen L, Toubro S, Hansen SM, Eildal JN, Bond AD, Bogeso KP, Bang-Andersen B, Kristensen AS, et al. Molecular Determinants for Selective Recognition of Antidepressants in the Human Serotonin and Norepinephrine Transporters. Proc. Natl. Acad. Sci. U.S.A. 2011; 108(29):12137–12142. [PubMed: 21730142]
19. Paczkowski FA, Sharpe IA, Dutertre S, Lewis RJ. Chi-Conotoxi and Tricyclic Antidepressant Interactions at the Norepinephrine Transporter Define a New Transporter Model. J. Biol. Chem. 2007; 282(24):17837–17844. [PubMed: 17428804]
20. Manepalli S, Geffert LM, Surratt CK, Madura JD. Discovery of Novel Selective Serotonin Reuptake Inhibitors through Development of a Protein-based Pharmacophore. J. Chem. Inf. Model. 2011; 51(9):2417–2426. [PubMed: 21834587]
21. Gabrielsen M, Ravna AW, Kristiansen K, Sylte I. Substrate Binding and Translocation of the Serotonin Transporter Studied by Docking and Molecular Dynamics Simulations. J. Mol. Model. 2012; 18(3):1073–1085. [PubMed: 21670993]
22. Sucic S, Dallinger S, Zdrazil B, Weissensteiner R, Jorgensen TN, Holy M, Kudlacek O, Seidel S, Cha JH, Gether U, et al. The N terminus of Monoamine Transporters is a Lever Required for the Action of Amphetamines. J. Biol. Chem. 2010; 285(14):10924–10938. [PubMed: 20118234]
23. Manepalli S, Surratt CK, Madura JD, Nolan TL. Monoamine Transporter Structure, Function, Dynamics, and Drug Discovery: A Computational Perspective. AAPS. J. 2012; 14(4):820–831. [PubMed: 22918625]
24. Caplan DA, Subbotina JO, Noskov SY. Molecular Mechanism of Ion-Ion and Ion-Substrate Coupling in the Na.- Dependent Leucine Transporter LeuT. Biophys. J. 2008; 95(10):4613–4621. [PubMed: 18708457]
25. Noskov SY, Roux B. Control of Ion Selectivity in LeuT: Two Na. Binding Sites with Two Different Mechanisms. J. Mol. Biol. 2008; 377(3):804–818. [PubMed: 18280500]
26. Zhao C, Stolzenberg S, Gracia L, Weinstein H, Noskov S, Shi L. Ion-Controlled Conformational Dynamics in the Outward- Open Transition from an Occluded State of LeuT. Biophys. J. 2012; 103(5):878–888. [PubMed: 23009837]
27. General IJ, Liu Y, Blackburn ME, Mao W, Gierasch LM, Bahar I. ATPase Subdomain IA Is a Mediator of Interdomain Allostery in Hsp70 Molecular Chaperones. PLoS Comput. Biol. 2014; 10:e1003624. [PubMed: 24831085]
28. Atilgan C, Atilgan AR. Perturbation-Response Scanning Reveals Ligand Entry-Exit Mechanisms of Ferric Binding Protein. PLoS Comput. Biol. 2009; 5:e1000544. [PubMed: 19851447]
29. Eyal E, Yang LW, Bahar I. Anisotropic Network Model: Systematic Evaluation and a New Web Interface. Bioinformatics. 2006; 22:2619–2627. [PubMed: 16928735]
30. Kazmier K, Sharma S, Quick M, Islam SM, Roux B, Weinstein H, Javitch JA, Mchaourab HS. Conformational Dynamics of Ligand-Dependent Alternating Access in LeuT. Nat. Struct. Mol. Biol. 2014; 21:472. [PubMed: 24747939]
31. Gür M, Zomot E, Cheng MH, Bahar I. Energy Landscape of LeuT from Molecular Simulations. J. Chem. Phys. 2015; 143:243134. [PubMed: 26723619]

32. Thomas JR, Gedeon PC, Madura JD. Structural Dynamics of the Monoamine Transporter Homolog LeuT from Accelerated Conformational Sampling and Channel Analysis. Proteins: Struct., Funct., Genet. 2014; 82:2289–2302. [PubMed: 24753369]

33. Gedeon PC, Thomas JR, Madura JD. Accelerated Molecular Dynamics and Protein Conformational Change: a Theoretical and Practical Guide Using a Membrane Embedded Model Neurotransmitter Transporter. Methods Mol. Biol. 2015; 1215:253–287. [PubMed: 25330967]

34. Chemical Computing Group. Molecular Operative Environment (MOE), 2008, 10. 1255 University Street, Suite 1600, Montreal, Quebec, Canada H3B 3X3: 2008.

35. Brooks BR, Bruccoleri RE, Olafson B, States DJ, Swaminathan S, Karplus M. CHARMM: A Program for Macromolecular Energy, Minimization, and Dynamics Calculations. J. Comput. Chem. 1983; 4:187–217.

36. Case, DA., Cheatham, TE., III, Simmerling, CL., Wang, J., Duke, RE., Luo, R., Merz, KM., Pearlman, DA., Crowley, M., Walker, RC., et al. AMBER 9. University of California; San Francisco, CA: 2006.

37. Rudnick GB. Cytoplasmic Permeation Pathway of Neurotransmitter Transporters. Biochemistry. 2011; 50:7462–7475. [PubMed: 21774491]

38. Phillips JC, Braun R, Wang W, Gumbart J, Tajkhorshid E, Villa E, Chipot C, Skeel RD, Kalé L, Schulten K. Scalable Molecular Dynamics with NAMD. J. Comput. Chem. 2005; 26:1781–1802. [PubMed: 16222654]

39. MacKerell AD Jr, Bashford D, Bellott M, Dunbrack RL Jr, Evanseck JD, Field MJ, Fischer S, Gao J, Guo H, Ha S, et al. All-Atom Empirical Potential for Molecular Modeling and Dynamics Studies of Proteins. J. Phys. Chem. B. 1998; 102:3586–3616. [PubMed: 24889800]

40. Feller SE, MacKerell ADJ. An Improved Empirical Potential Energy Function for Molecular Simulations of Phospholipids. J. Phys. Chem. B. 2000; 104:7510–7515.

41. Wang J, Wolf RM, Caldwell JW, Kollman PA, Case DA. Development and testing of a general AMBER force field. J. Comp. Chem. 2004; 25:1157–1174. [PubMed: 15116359]

42. Dupradeau FY, Pigache A, Zaffran T, Savineau C, Lelong R, Grivel N, Lelong D, Rosanski W, Cieplak P. The R.E.D. tools: Advances in RESP and ESP Charge Derivation and Force Field Library Building. Phys. Chem. Chem. Phys. 2010; 12:7821–7839. [PubMed: 20574571]

43. Hamelberg D, Mongan JJ, McCammon JA. Accelerated Molecular Dynamics: a Promising and Efficient Simulation Method for Biomolecules. J. Chem. Phys. 2004; 120:11919–29. [PubMed: 15268227]

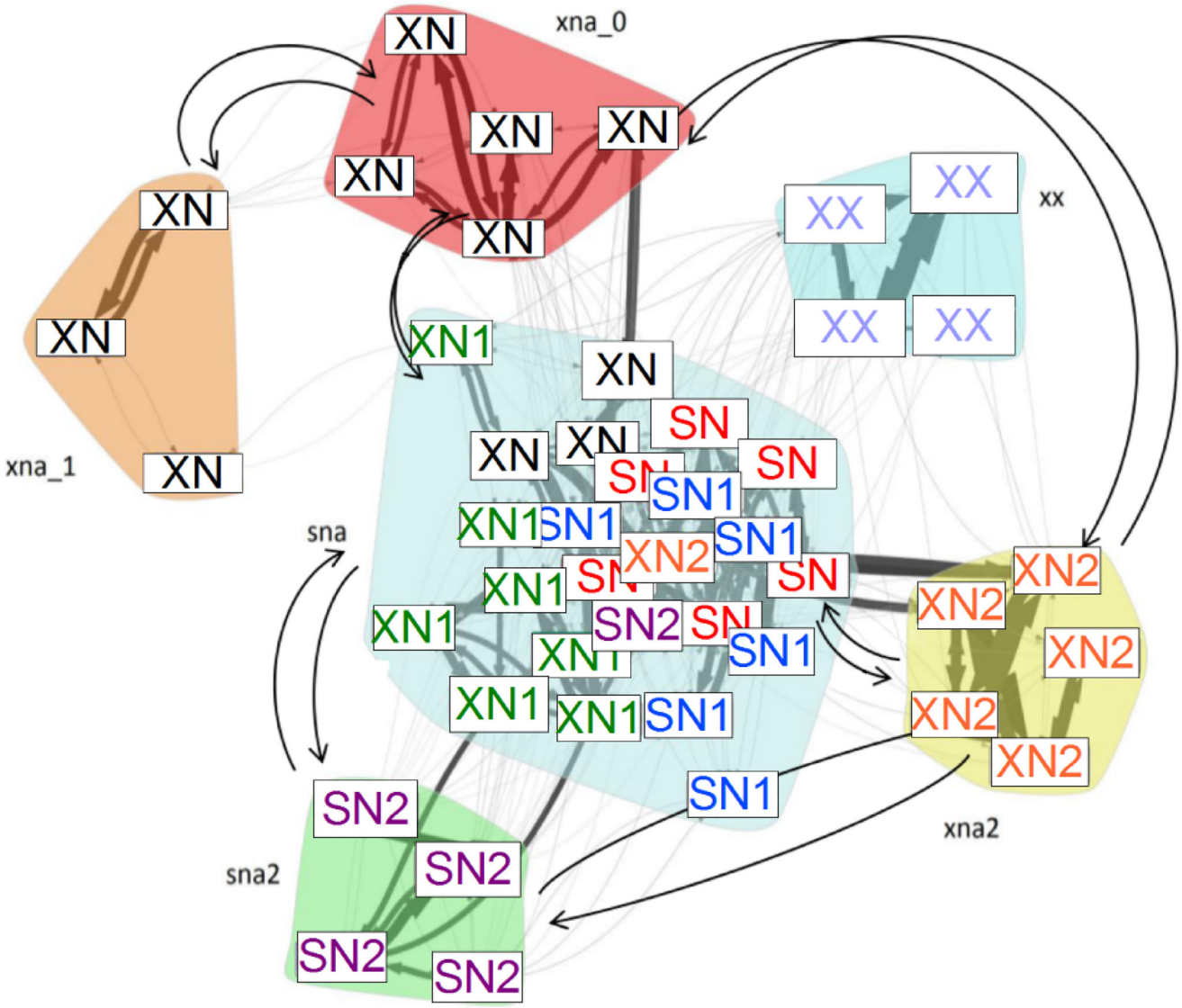

Figure 1.

Microstates generated with hybrid clustering lumped into six macrostates. Each microstate is labeled in capital letters by the environment where it belongs. Terminology: X = no substrate, S = substrate, N1 = $Na1^+$, N2 = $Na2^+$, N = both ions. Macrostates are labeled in lower case, and the labeling is related with the environment they represent. The two macrostates representing the XN environment are called xna_0 and xna_1, the most populated is sna, and the remaining three are xx, xna2, and sna2. Arrows indicate transitions between states. Higher flux is represented by wider arrows.

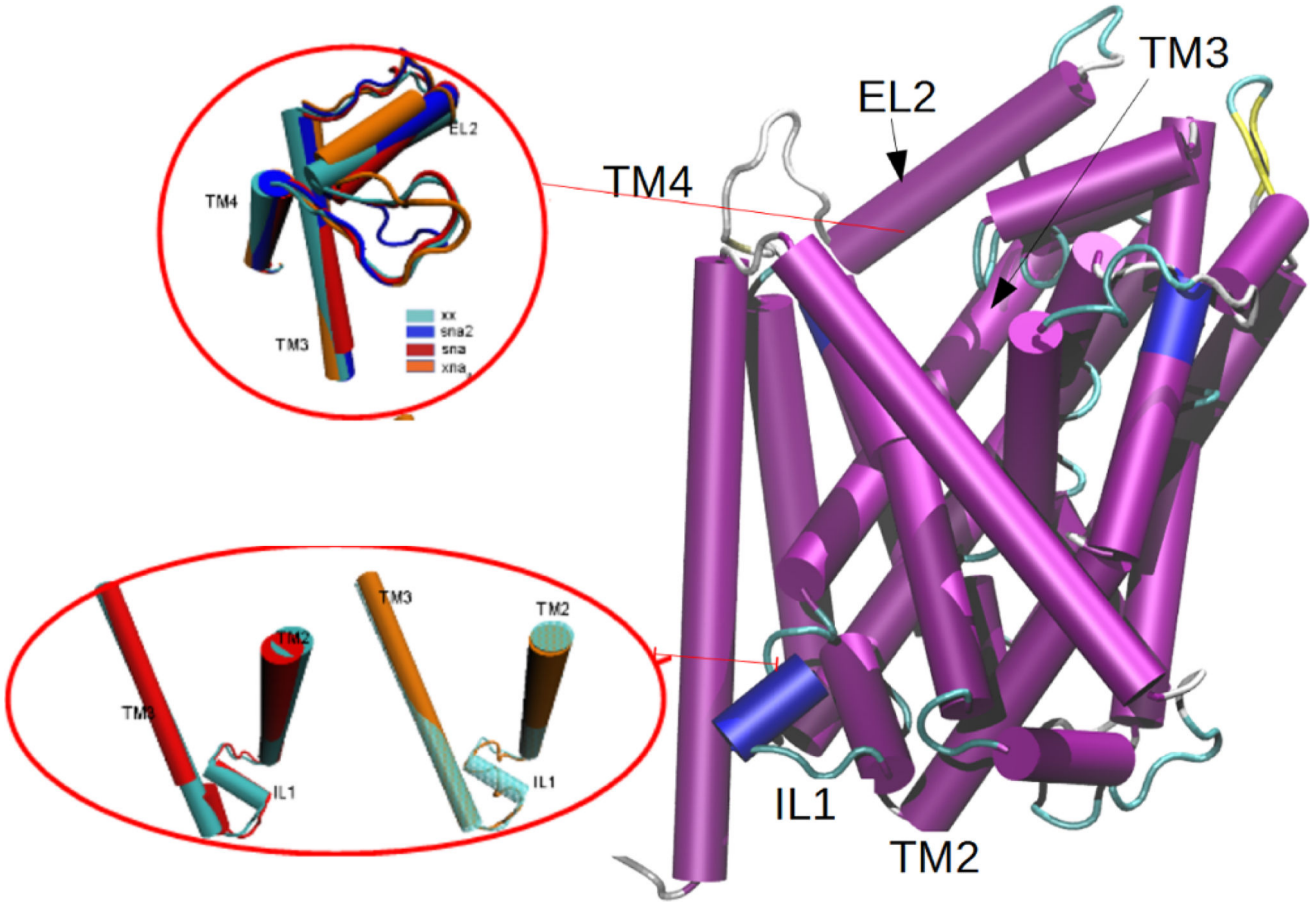

Figure 2.

Extracellular loop 2 (EL2) connecting TM3 and TM4 helices for xx macrostate (cyan), xna_0 (orange), and sna1 (blue) (top). Intracellular loop IL1 connecting TM2 and TM3 for macrostates sna (red) and xx (cyan) (bottom left) and macrostates xna_0 (orange) and xx (cyan) (bottom right).

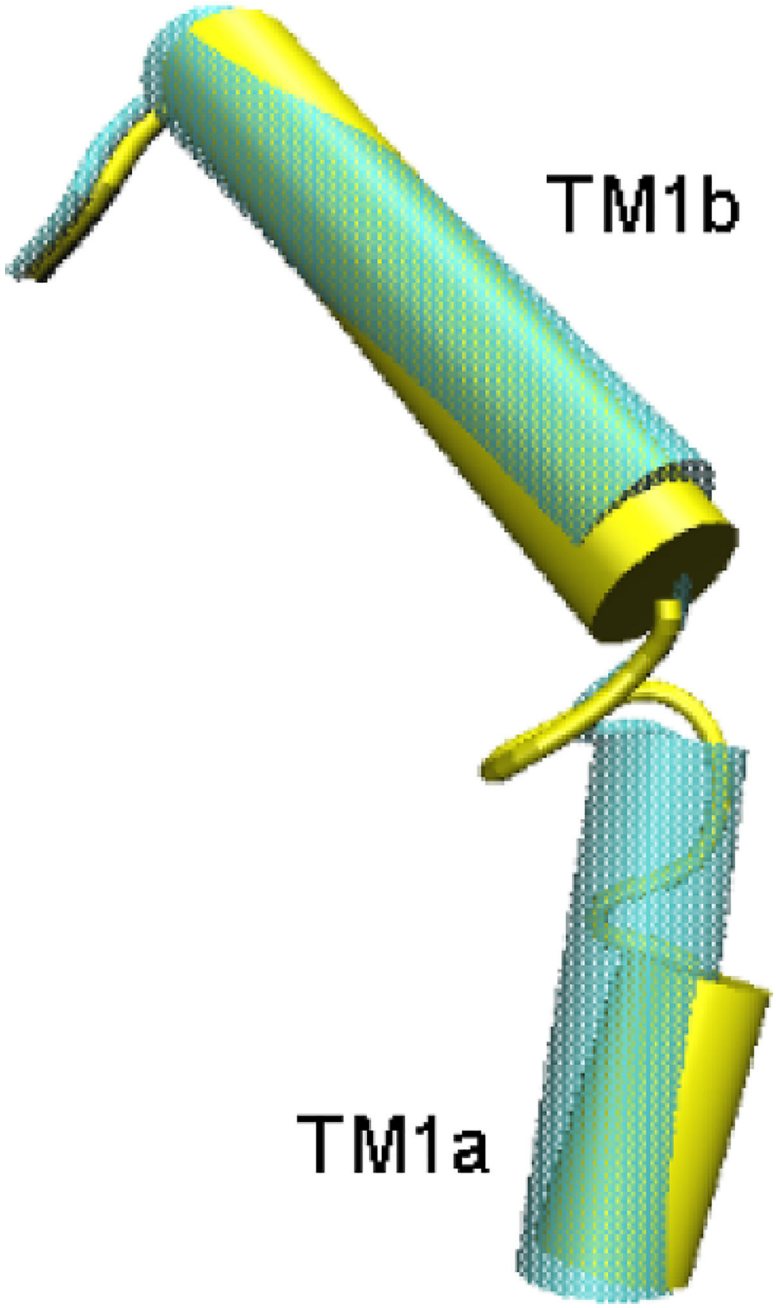

Figure 3.
TM1a and TM1b helices for macrostate xna2 (yellow) compared with xx (cyan).

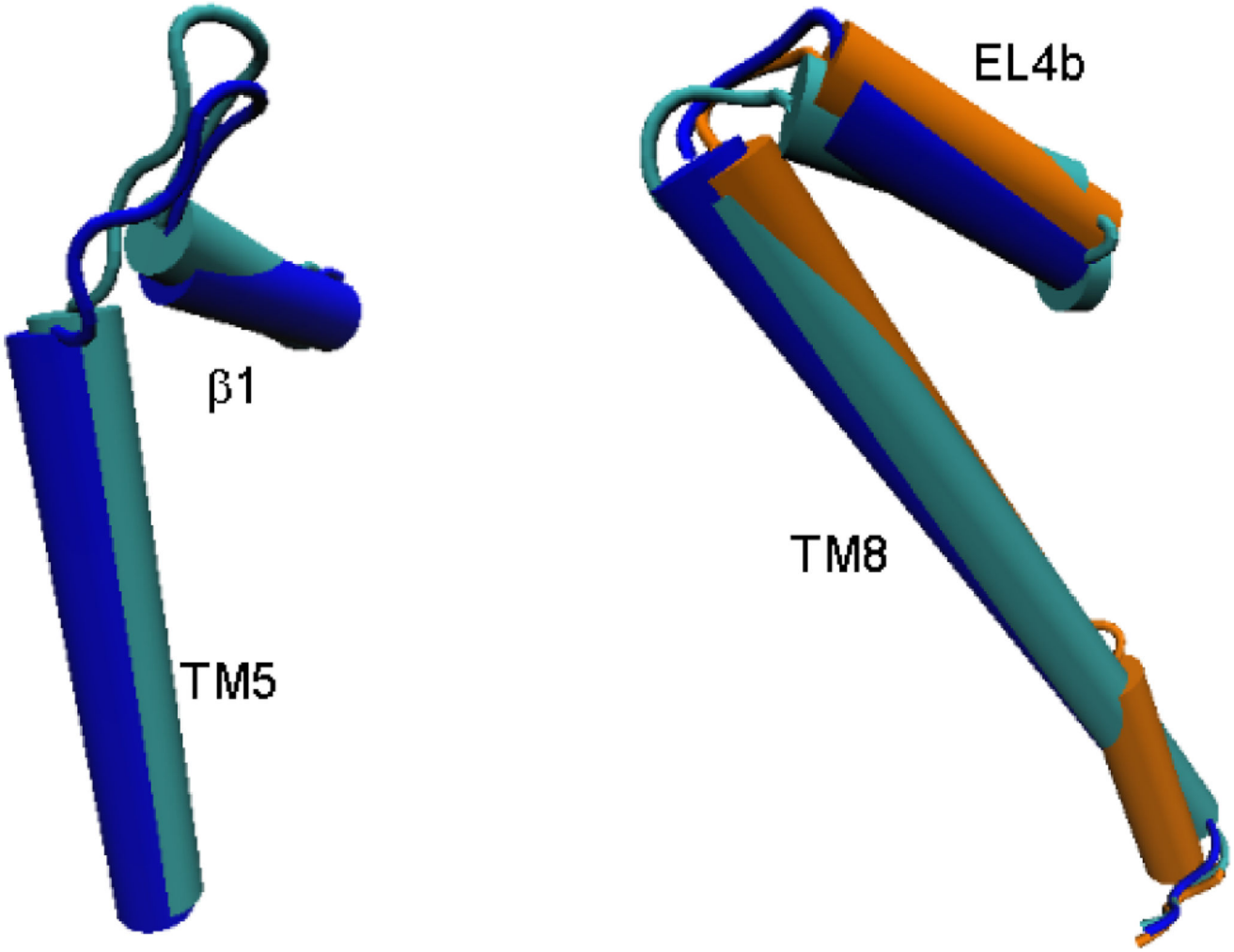

Figure 4.
TM5 helix and β_1 for macrostate sna2 (blue) compared to xx (cyan) (left). TM8 and EL4b for xna_0 (orange), sna2 (blue) compared with xx (cyan) (right).

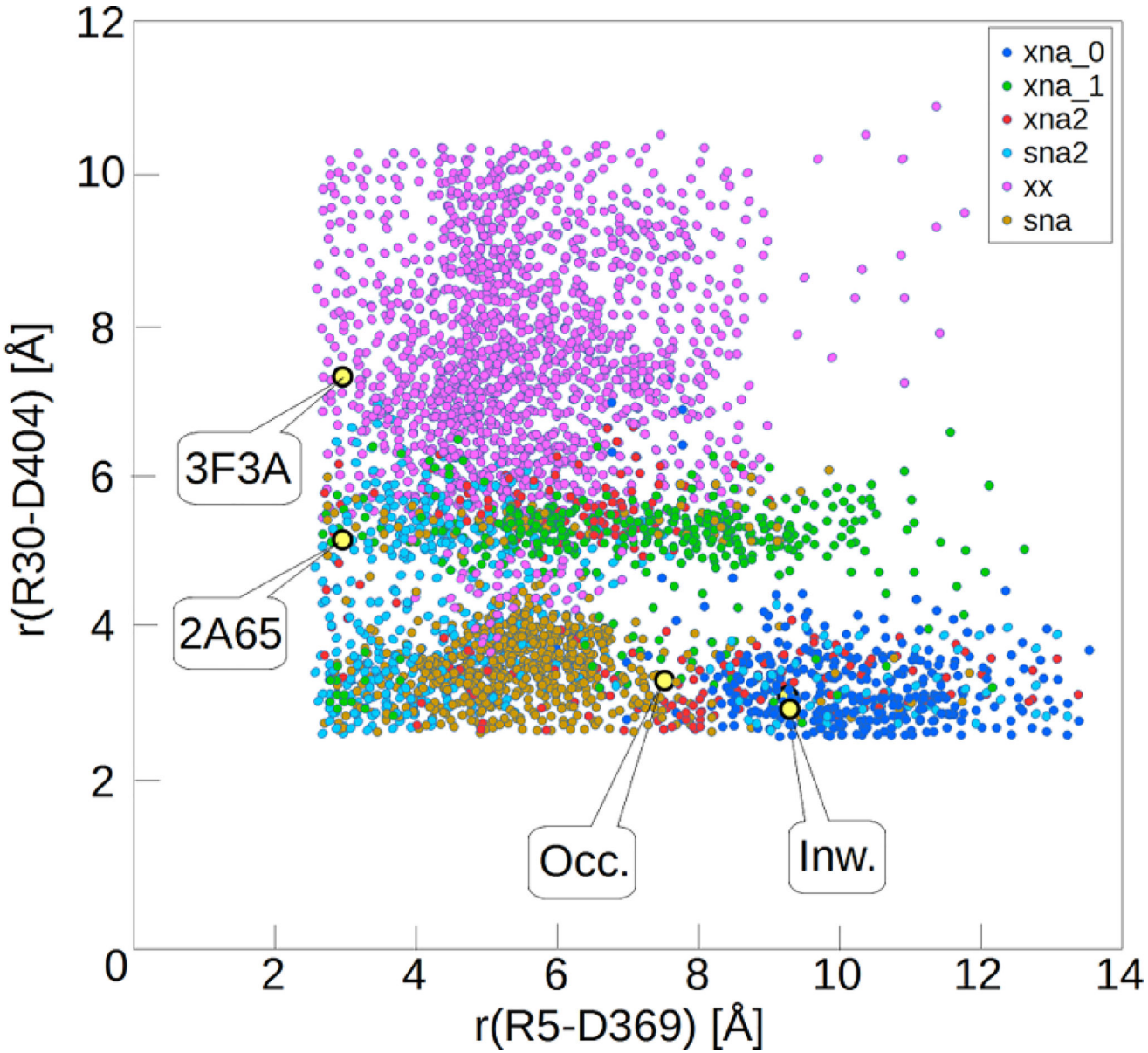

Figure 5.

Intra- and extracellular distances represented by R5–D369 and R30–D404 distances, respectively, sampled by the six macrostates. The locations of previously reported coordinates are shown for comparison.

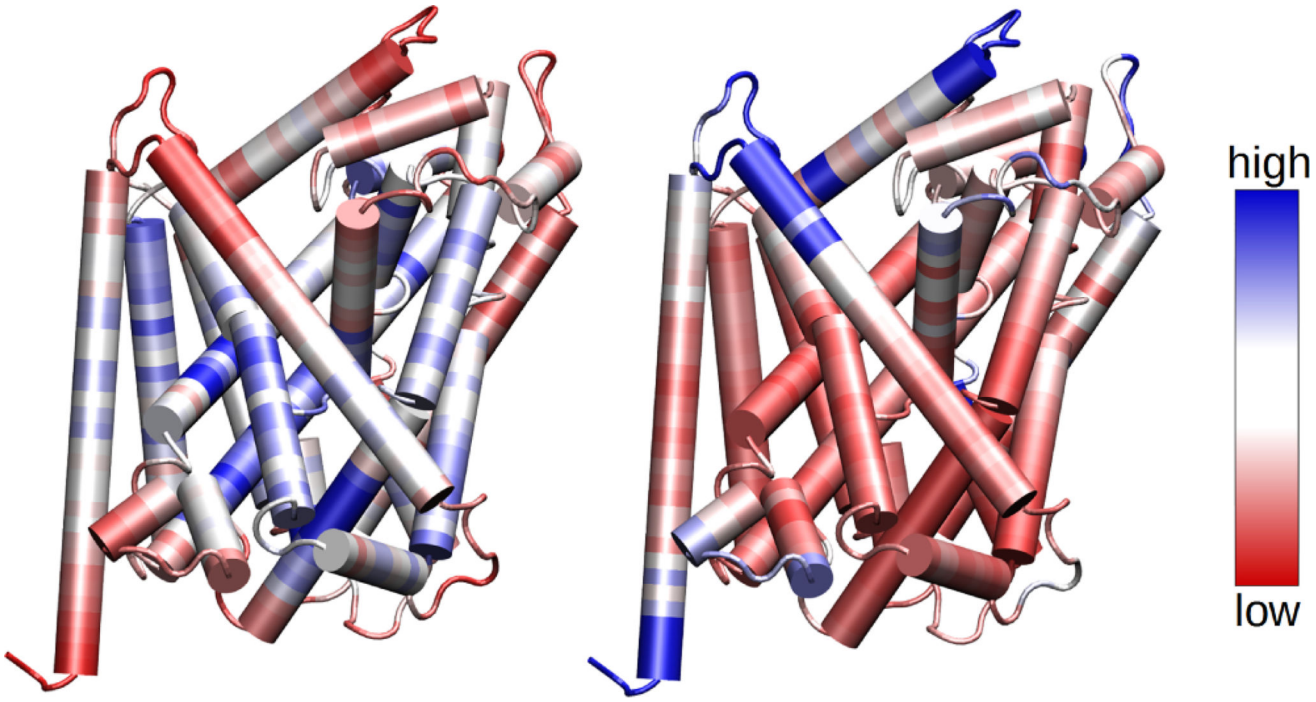

Figure 6.

LeuT colored by influence (left) and sensitivity (right) PRS values of each residue, averaged over the XX, XN1, XN2, XN, SN1, SN2, and SN environments. The scale goes from red (low) to blue (high) values.

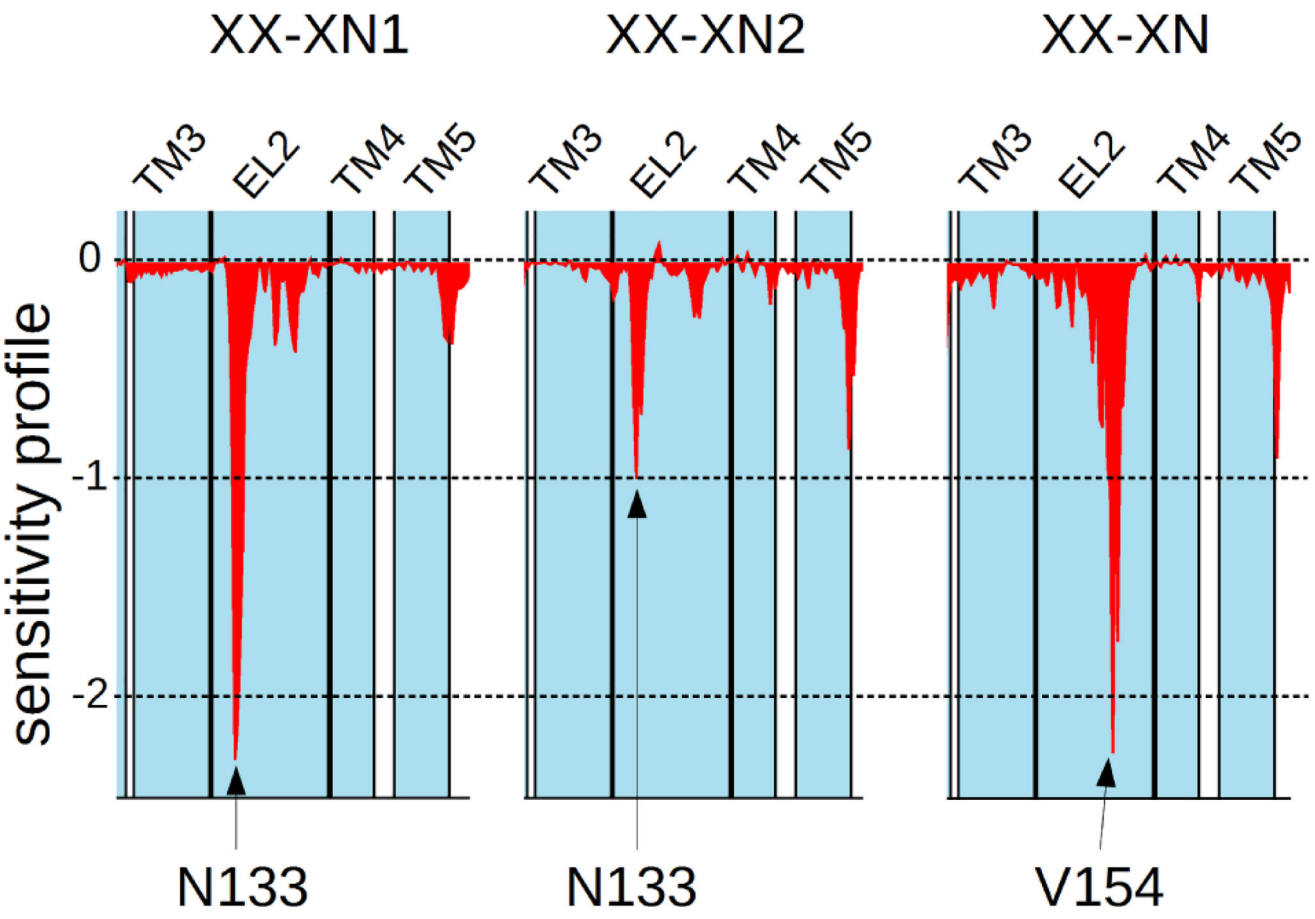

Figure 7.
Sensitivity profile around EL2 corresponding to the difference between XX and XN1, XN2, and XN.

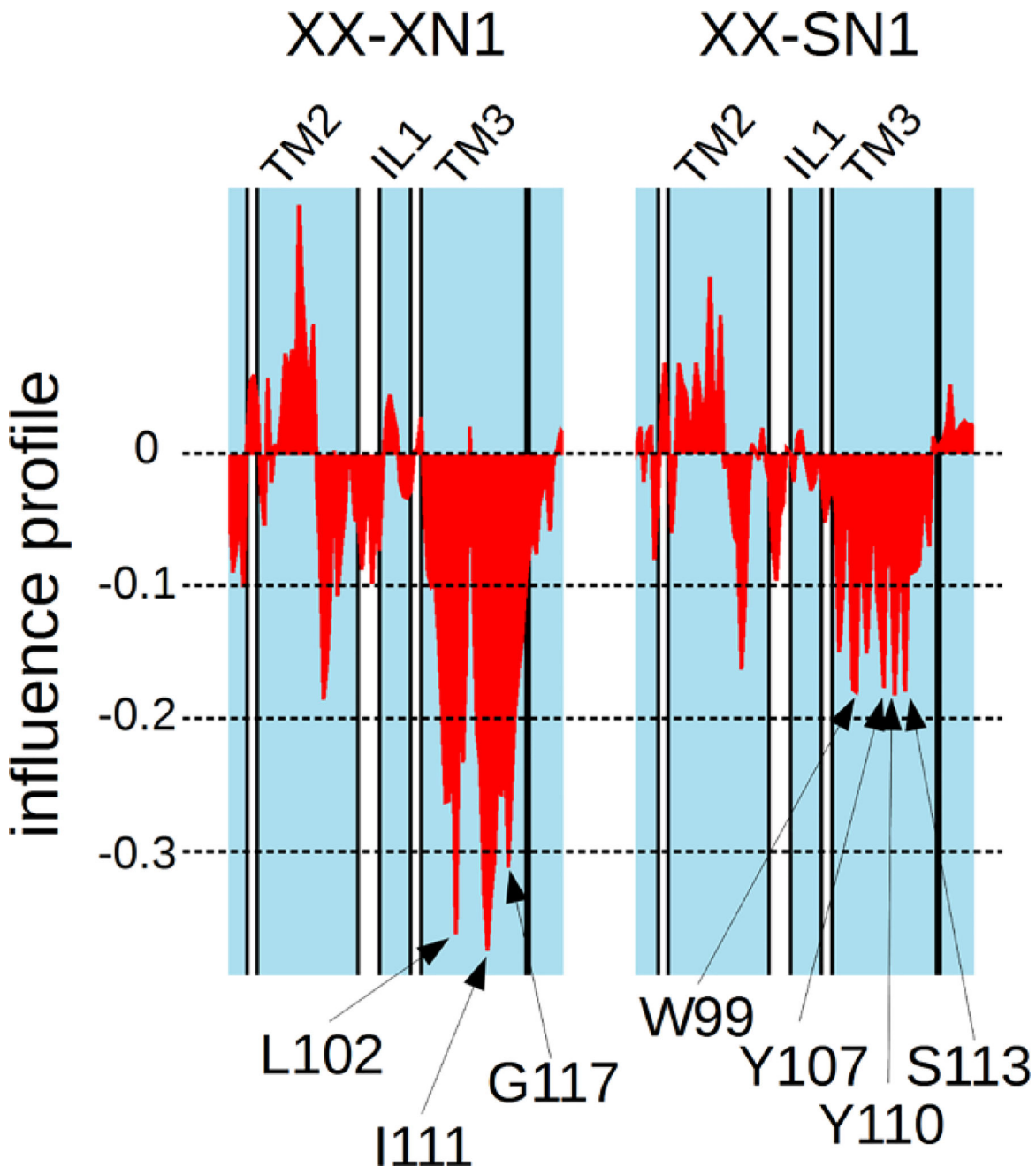

Figure 8.
Influence profile around IL1 corresponding to the difference between XX, XN1, and SN1.

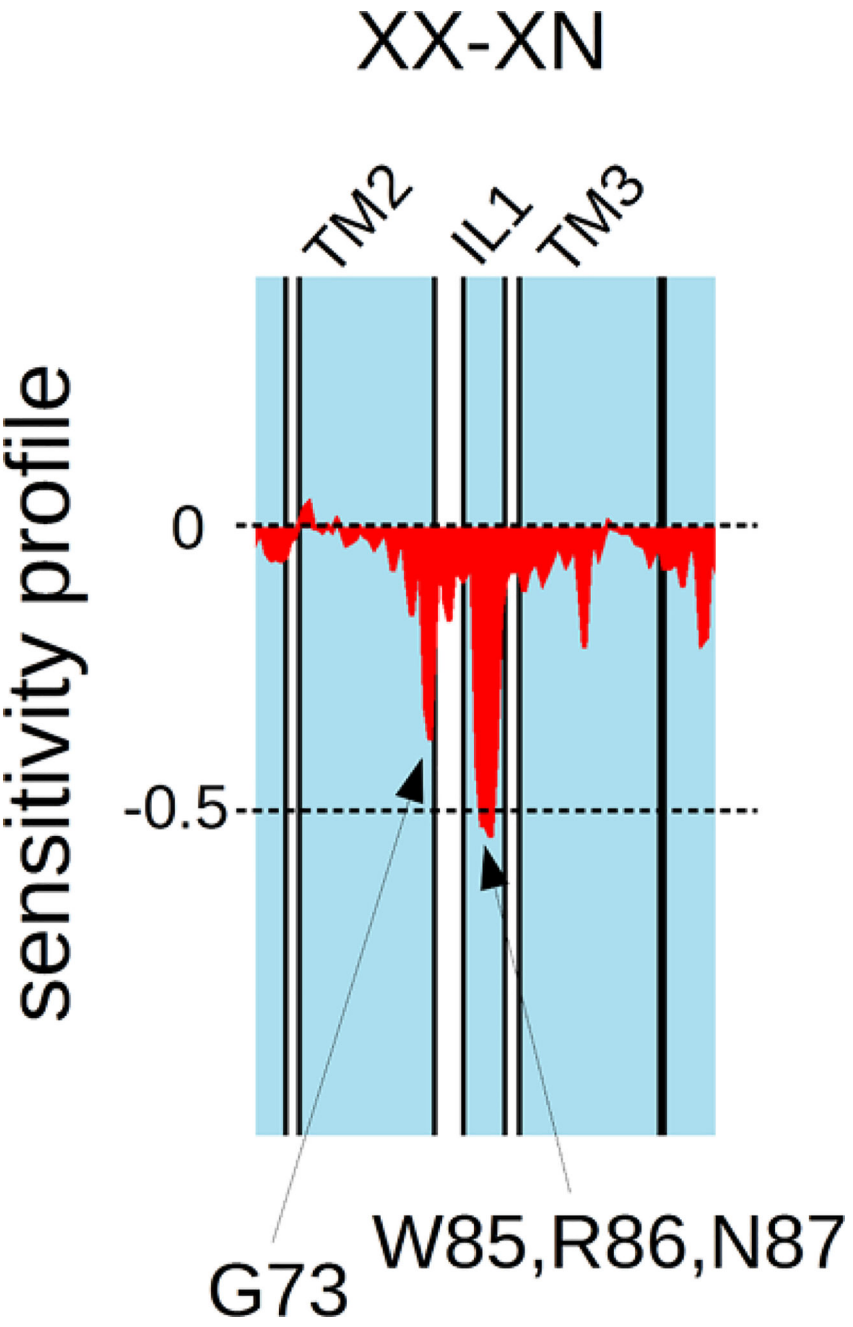

Figure 9.
Sensitivity profile around IL1 corresponding to the difference between XX and XN.

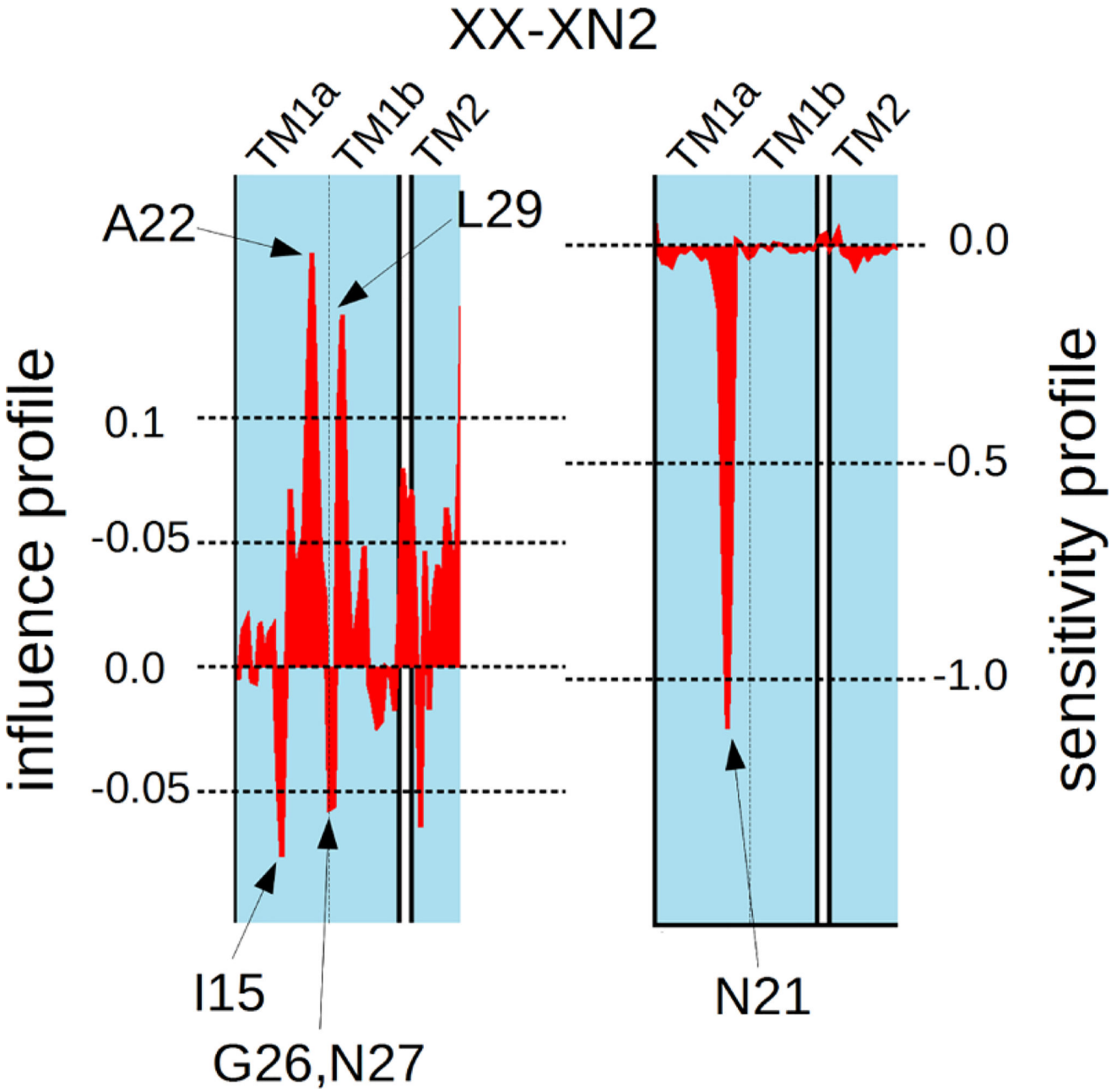

Figure 10.
Influence profile around TM1 corresponding to the difference between XX and XN2.

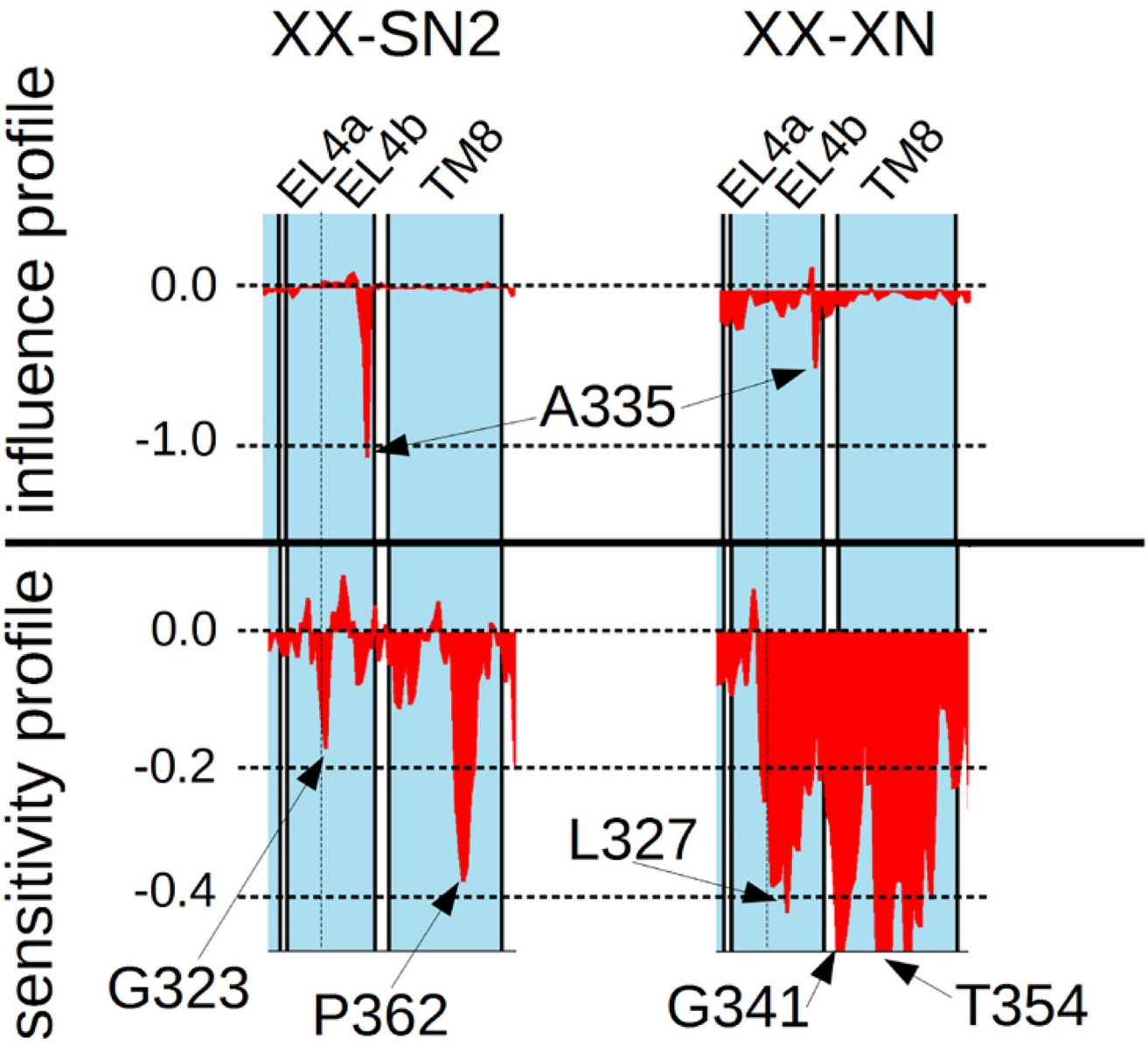

Figure 11.
Sensitivity and influence profiles around EL4 corresponding to the difference between XX, XN, and SN2.